Beltran-Osuna, AA.; Gómez Ribelles, JL.; Perilla, JE. (2020). Temperature and ph responsive behaviour of antifouling zwitterionic mesoporous silica nanoparticles. Journal of Applied Physics. 127(13):135106-1-135106-11. https://doi.org/10.1063/1.5140707

TEMPERATURE AND pH RESPONSIVE BEHAVIOR OF ANTIFOULING ZWITTERIONIC pSBMA-MSN NANOPARTICLES

Ángela A. Beltrán-Osuna[1], Jairo E. Perilla[1,*], José L. Gómez-Ribelles[2]

[1] Grupo de Procesos Químicos y Bioquímicos, Departamento de Ingeniería Química y Ambiental, Universidad Nacional de Colombia, 111321 Bogotá, Colombia

[2] Centre for Biomaterials and Tissue Engineering, Universitat Politècnica de València, 46071 Valencia, Spain

[3] Biomedical Research Networking Center in Bioengineering, Biomaterials and Nanomedicine (CIBER-BBN), Valencia, Spain

* Author to whom correspondence should be addressed: jeperillap@unal.edu.co

Abstract

Zwitterionic polymer brush grafting is considered as a serious strategy for surface modification on mesoporous silica nanoparticles (MSN), and a prominent alternative to polyethylene glycol (PEG) films for antifouling applications. In this study, the solution behavior of poly(sulfobetaine methacrylate) (pSBMA) polymer brushes grafted on MSN (95 ± 15 nm particle diameter, 2.8 nm pore size) was evaluated. The temperature-responsive layers increased their hydrodynamic diameter (d_H), indicating a conformational change from a surface-collapsed state to a fully solvated brush. This development was clearly marked by a transition temperature, directly related to the molecular weight and theoretical length of the polymer chains. Variation of the d_H with pH values was also studied and a zwitterionic range of 5-9 was stablished where the electric charges in the molecule were balanced. Additionally, zeta potential (ZP) values for all pSBMA-MSN products were also measured. A decreasing trend of ZP with pH and an isoelectric point around 5.5-6.5 was obtained for all dispersions. Furthermore, the influence of temperature was analyzed on ZP and a directly proportional correlation was found, with increasing rates of 0.50-0.87 %/°C. Finally, ZP variation with electrolyte concentration was determined and a range of 40-60 mM of NaCl concentration was established to reach an almost zero charge point for all nanoparticles. It was demonstrated that solution response of pSBMA-MSN products can be modulated by the temperature, pH and ionic concentration of the media. These behaviors could be used as controlled release mechanisms for the application of pSBMA-MSN as a carrier in biomedicine and nanophamaceutical fields in the future.

Keywords

MSN, nanoparticles, pSBMA, zwitterionic, antifouling

I. INTRODUCTION

Nanotechnology is undoubtedly one of the most powerful tools in present-day in a variety of fields such as electronics, environment, health and medicine. Nanocarriers are being considered as compelling platforms for all sorts of applications, including biosensors, microfluidics, biomolecule detection and cell sorting, tissue engineering, imaging, drug delivery and nanobiotechnology [1,2]. As drug delivery systems, nanocarriers should resolve critical issues of conventional drug treatments, such as rapid clearance, uncontrollable release and low bioavailabity [3]. Thus, three main characteristics are desirable in a carrier: high load capacity, “stealth” long circulation and a responsive mechanism to achieve a controlled drug delivery [4]. Two options of silica particles (<200 nm diameter) are usually available, silica nanoporous nanoparticles (SNP, < 2nm pore size) and mesoporous silica nanoparticles (MSN, 2-50 nm pore size). Particularly, MSN are widely known for their high surface areas (10-1280 m^2) [5]. Accordingly, MSN are promissory vehicles due to their higher load capacity, biocompatibility, and tunable pore sizes [6]. However, MSN always aggregate and burst drug release, limiting the application of unmodified MSN as drug carriers [7,8]. Nowadays, only two SNP systems are going through clinical trial phases, while MSN are not FDA approved yet [9], which makes the studies on the MSN surface modification highly relevant.

Nonspecific protein adsorption is generally accepted as the first step for microbial adhesion, further resulting in biofilm formation [10]. This protein adsorption would lead to nanoparticle aggregation, which is one of the major challenges in biomedical applications [11]. For example, to avoid particle aggregation and, therefore, to attain “stealth” properties, MSN could be coated with a polymer brush, to achieve particle stabilization, besides improving delivery kinetics and release performance. Polyethylene glycol (PEG) has been considered for a long time as the reference material for surface functionalization in order to avoid protein adhesion. PEGylated nanoparticles have been reported to render a neutrally-charged surface, reducing adhesion by preventing electrostatic interactions [12]. However, largely PEGylated SNP systems have reported to have a highly variable cancer-targeted delivery efficiencie [13]. One of the best alternatives is the use of zwitterionic polymers, which are amphiphilic macromolecules possessing both cationic and anionic groups within the same repetitive unit (polybetaines) or along the same backbone (polyampholytes)

[3,12,14]. Zwitterions have similar properties to PEG, reducing nanocarrier recognition with an intrinsic ion paring mechanism. This allows the formation of a strong hydrated layer which prevents protein adsorption more efficiently than PEG [4,15–17]. For example, preparation of ultra-low-fouling or antifouling surfaces can be achieved by grafting zwitterionic polybetaines, such as poly(sulfobetaine methacrylate) (pSBMA) and poly(carboxybetaine methacrylate) (pCBMA), which lead to fibrinogen adsorption levels as low as < 0.3 ng/cm^2 [10]. Hence, zwitterionic materials have exceptional potential in drug delivery, as nanoparticle stabilizers and antifouling coatings [14]. Nonetheless, there is a lack of studies for the application of these polymers in drug carriers [12]. A patent is currently active claiming the preparation of core-shell zwitterionic polybetaine-coated nanoparticles, including cores such as silica, gold, iron oxide, carbon nanotube, polystyrene, silicone, quantum dots and also nanogels, among others [18].

The morphological characteristics of the polymer brush (*e.g.*, graft density and thickness) are fundamental to the antifouling efficiency of the coating layer and "stealth" capacity of the nanocarrier [4]. Among many living polymerization techniques, atom transfer radical polymerization (ATRP) is preferred to manipulate brush thickness by means of the molecular weight, allowing the control over the whole architecture [19]. In consequence, the solution behavior of the polymer brush can also be finely tuned to respond to environmental conditions like pH, temperature or ionic strength, which also affect the antifouling capacity of the coatings [2]. There are two important phenomena that define the solution behavior of free zwitterionic polymer chains. On the one hand, there is the existence of an upper critical solution temperature (UCST), at which the polymer undergoes a hydrophobic-hydrophilic phase transition, explained by the dipole-dipole interactions between the betaine groups [20]. Thus, at temperatures above the UCST, the zwitterionic chain remains miscible, while at lower temperatures, phase separation occurs. On the other hand, zwitterionic polymers also exhibit the antipolyelectrolyte effect that allows polybetaines and polyampholytes to increase inter- and intra-chain electrostatic attractions in the presence of a salt. Thereby, the zwitterionic becomes more soluble at certain electrolyte concentration, owing to the destabilization of the zwitterionic complexes [14]. The analysis of these phenomena whilst zwitterionic chains are attached to MSN surface are necessary to properly understand the solution behavior

of the nanocarrier. For example, nanoparticles smaller than 100 nm and nearly neutrally charged (±10 mV) have shown higher delivery efficiencies for cancer targeted therapy [13]. In this trend, more studies evaluating the influence of solution conditions such as pH, temperature or salt content, on the particle diameter and zeta potential, are imperative to properly asses the nanocarrier properties for each application.

A variety of zwitterionic self-assembled polymer structures has been proposed, including thermo-responsive coil-blub pCBMA copolymers (200-600 nm diameter) for biomaterial design [21], chitosan-pSBMA micelles (200-300 nm diameter) for supporting biological activities of membrane-active peptides [22], and thermo- and pH-responsive pSBMA copolymer microassemblies (10-1165 nm diameter) for oral delivery [23]. Zwitterionic polymers have been also used for surface modification of microparticles of different nature. On the one hand, polystyrene (PS) microbeads (2.8 μm diameter) have been functionalized with a sulfobetaine polymer to be used in mass spectrometry-based proteomics [2], and also in synthesized sulfobetaine-functionalized PS colloidal spheres (367 ± 18 nm) for tunable and responsive photonic crystals arrays [24]. On the other hand, colloidal SNP (1-1000 nm) have been used for diagnosis and biosensing devices, including pCMB-SNP colloidal crystals (280 nm diameter) [25], pSBMA-SNP carriers (50 nm diameter) [26], lysine-SNP (80 nm) as additives for ultrafiltration membrane improvement [27], and amino acid-based SNP (30 nm diameter) for biomolecule immobilization or biofunctional surface preparation [11]. Nevertheless, the antifouling capacity of zwitterionic SNP was determined only until recent years, *e.g.*, SNP (7-75 nm) coated with a polysulfobetaine showed an adsorption reduction of 91% of bovine serum albumin (BSA) protein [17]. Furthermore, very few reports were found for nanocarriers that would include the advantages of both MSN and zwitterionic polymers for drug delivery applications. Those nanosystems were especially proposed for cancer therapy, *e.g.*, PEG-derivated phospholipid-functionalized MSN (200 nm diameter) [28], thermo-responsive polysulfobetaine copolymer-MSN (100 nm diameter) [29], charge-switchable MSN functionalized with carboxylic and quaternary amine zwitterionic moieties (150 nm) [30] and Fe_3O_4-MSN-methylchloropropionate core-shell nanoparticles (70 nm diameter). However, none of these studies reports the influence of the morphological brush features on protein adhesion.

In a recent study [31] , the antifouling capacity of pSBMA-MSN carriers was determined. For that purpose, well-shaped monodispersed spherical MSN (95 ± 15 nm particle diameter, 2.8 nm pore diameter) were surface functionalized with an ATRP initiator (BrTEOS). Next, pSBMA was grafted from BrTEOS-MSN by the ATRP technique. Two morphological brush characteristics, graft density and thickness, were controlled by varying the reaction time with BrTEOS during functionalization, and the monomer/catalyst molar ratio during polymerization. Protein adsorption was measured in the different zwitterionic brushes prepared, which reduced by 96% and 76% the adhesion of fibronectin and BSA proteins, respectively. In this study, the solution behavior of those pSBMA-MSN products was evaluated. Aqueous dispersions of all samples are prepared and analyzed by dynamic light scattering (DLS) technique. In order to understand the zwitterionic brush conformation in solution, pH and temperature of media was varied and the hydrodynamic diameter (d_H) was measured for all dispersions. In addition, the influence of temperature, pH and ionic concentration of the media was analyzed by measuring the zeta potential (ZP). This study could help to deeply understand the responsive behavior of zwitterionic layers on curved-nanoscale surfaces, to be used as possible control mechanisms for the application of pSBMA-MSN as carriers in biomedicine.

II. EXPERIMENTAL PROCEDURES

A. Materials

Monodispersed spherical mesoporous silica nanoparticles (MSN), of 95 ± 15 nm of diameter and a pore size of 2.8 nm were synthesized and coated with poly(sulfobetaine methacrylate) (pSBMA), as previously reported [31,32]. Briefly, MSN were synthesized using tetraethyl orthosilicate (TEOS) as a silica precursor, and hexadecyltrimethylammonium bromide (CTAB) as a surfactant template. First, 1 g of CTAB was added to 480 mL of water, and mixed with 3.5 mL of NaOH aqueous solution (2 M). After complete dissolution, 5 mL of TEOS were added dropwise and reaction took place at 80°C and 500 rpm during 2 hours. MSN particles were recovered from medium by several centrifugation and washing cycles, using distilled

water until reaching a neutral pH value, and finally calcined to remove the template. Then, MSN were functionalized with the initiator 2-bromo-2-methyl-N-3-[(triethoxysilyl)propyl]-propanamide (BrTEOS), and coated with the zwitterionic polymer by a living polymerization technique, such as atom transfer radical polymerization (ATRP). Synthesis of different polymer brushes was performed by modifying two variables: functionalization time of MSN with BrTEOS and molar ratio between monomer and catalyst (SBMA/CuBr) during ATRP reaction. Nine different products were obtained (pSBMA-MSN) with variety of morphologies, as summarized in Table I.

Table I. Summary of ATRP reaction conditions for the synthesis of pSBMA-MSN products.

	BrTEOS-MSN	**pSBMA-MSN**		**pSBMA**		
ATRP	Reaction BrTEOS (h)	SBMA/CuBr molar ratio	Graft density (molecules/nm^2)	PDI	$\bar{M}_n$	Theoretical chain length (nm)
1	0.5	50	0.16	1.01	22 000	11
2	4	50	0.41	1.29	11 400	8
3	12	50	0.32	1.36	15 000	10
4	24	50	0.18	1.55	25 400	18
5	1	5	0.15	1.08	6 500	4
6	1	25	0.25	1.17	13 000	8
7	1	50	0.27	1.42	15 300	11
8	1	100	0.35	1.44	15 300	11
9	1	150	0.51	1.33	32 300	20

Distilled water, NaCl (>99.0%, ACS, Sigma-Aldrich), HCl (0.1 M) and NaOH (0.1 M) were used to analyze the behavior of pSBMA-MSN products in solution. Potentiometric pH measurements were made by a CyberScan pH ion 510 instrument, using standard buffers for a three-point calibration (4.01, 7.01, 9.21). Samples were pretreated by sonication using a Bandelin Sonorex Super RK103H. A ZetaSizer Nano ZS (Malvern Instruments Ltd.) with a 632.8 nm red laser was used to carry out both characterization techniques, dynamic light scattering (DLS) and zeta potential (ZP) as described below.

B. Hydrodynamic diameter determination

Dynamic light scattering (DLS) technique was used to determine the hydrodynamic diameter of the pSBMA-MSN products dispersed in water. ZetaSizer DLS software directly reports the size of particles, by using the Stokes-Einstein Equation:

$$d_H = k_B T/(6\pi\eta D) \quad (1)$$

where d_H is the hydrodynamic diameter (*nm*), k_B is the Boltzmann constant (1.38065×10^{-23} *J/K*), T is the temperature (*K*), η is the viscosity of the solvent (*kg/m·s*) and D is the diffusion coefficient (m^2/s). First, sample dispersions were prepared by adding 1 ± 0.1 mg of pSBMA-MSN to 1 mL ± 0.05 mL of water in a 2 mL Eppendorf, followed by a one-hour sonication period. Then, an aliquot was taken to achieve a final nanoparticle concentration of 0.025 mg/mL. Each sample was sonicated 5 minutes right before analysis. All particle size runs were made at 30°C, adding 1 mL sample dispersion in a polystyrene disposable cuvette. The final particle size value reported was the average value of the five replicas that were taken for each sample.

New sample dispersions of each product were prepared likewise to study the influence of temperature on the particle size. First, instrument temperature was kept at 15°C for 30 minutes before inserting the cuvette with the prepared sample. Then, other 15 minutes of waiting period were allowed for the cuvette to stabilize its temperature. Each particle size measurement took 10 minutes at a given temperature, after which the instrument temperature raised 1°C, allowing a 15-minute stabilization period between each measurement. Each product sample was analyzed varying the temperature from 15°C to 65°C, for a total test time of 21 hours per sample. Finally, another set of new sample dispersions was prepared to study the influence of pH value on the particle size. For each product, samples at different pH values (from 1 to 13) were prepared and sonicated as previously described. Then, pH value was verified by potentiometric measurements, before adding 1 mL sample dispersion into the cuvette for immediate analysis.

C. Zeta potential measurement

ZP values were determined by the ZetaSizer software, measuring the electrophoretic mobility μ_E defined by:

$$\mu_E = V/E \quad (2)$$

where V is the particle velocity and E the electric field intensity. Both, μ_E and ZP are related through Henry's Equation [33]:

$$\mu_E = 2\,\varepsilon\, ZP\, f(\kappa a)/\, 3\eta \quad (3)$$

where ε is the dielectric constant, η the solvent viscosity and $f(\kappa a)$ the Henry's function, depending on the particle radius (a) and the Debye length ($1/\kappa$), which can be calculated by the following equation [34]:

$$1/\kappa = \sqrt{\varepsilon_0 \varepsilon_r k_B T/(2000 e^2 I N_A)} \quad (4)$$

where ε_0 is the electric permittivity in vacuum (*8.854×10^{-12} C^2/Nm^2*), ε_r is the dielectric constant of the medium, k_B is the Boltzmann's constant (*1.38065×10^{-23} J/K*), *T* is the temperature (*K*), *e* the electron charge (C), *I* the ionic strength of the medium (*mol /L*), and N_A the Avogadro's constant (*6.023 x 10^{23}/mol*). Therefore, $f(\kappa a)$ can be defined by Ohshima's Equation [35]:

$$f(\kappa a) = 1 + 1/2(1 + \delta/\kappa a) \quad (5)$$

$$\delta = 2.5/(1 + e^{-\kappa a}) \quad (6)$$

The influence of pH, temperature and NaCl concentration on ZP measurements was analyzed in three series of experiments. First, aqueous solutions were prepared by adjusting their pH value from 1 to 13 by using a potentiometer. These solutions were used immediately for the preparation of the different pSBMA-MSN dispersions, with a nanoparticle concentration of 1.0 mg/mL. A temperature stabilization period of 5 minutes was allowed for any cuvette before each measurement. The reported values

are the average of the three consecutive measurements performed for each product sample at a given pH value, using 180 internal scans of 3 seconds each, for a total test time of 9 minutes per sample. Likewise, ZP values were determined at neutral conditions (pH = 7) by changing the dispersion temperature from 15 to 65 °C, for each pSBMA-MSN product. Finally, NaCl solutions at different concentrations (from 0 to 100 mM) were used to prepare product dispersions using a nanoparticle concentration of 0.5 mg/mL, for the determination of ZP values at 30°C.

III. RESULTS AND DISCUSSION

A. Influence of temperature in hydrodynamic diameter

In order to study the behavior of the zwitterionic polymer layers in each of the nine pSBMA-MSN products, the hydrodynamic diameter (d_H) was measured by DLS, varying the temperature from 15°C to 65°C. First, ATRP products from 1 to 4 were analyzed as shown in Figure 1. A three-stage progression curve was observed in all cases. At the beginning, particle diameter remained constant, while temperature rose, until reaching a second stage where there was a fast increase in the hydrodynamic diameter. At the end of this stage, a peak temperature was reached and then, the particle diameter slowly decreased until reaching a final plateau of constant value. This conformational change of polymer chains could be related to the existence of the UCST that exhibit zwitterionic materials [36]. For pSBMA, the dependence of UCST on molecular weight has been already analyzed, reporting values from 28°C to 52°C for molecular weights between 56 000 and 307 0000 [37]. According to this report, a critical temperature below 28°C could be expected for the pSBMA here synthesized (Table 1). However, UCST is strictly defined for free polymer chains in solution, and higher energy requirements seem to be necessary for pSBMA attached to MSN particles, giving as a result higher transition temperatures as shown in Figure 1. This increment may also be related to the fact that grafted chains on silica allow higher pSBMA concentrations. It has been reported that UCST increases from 15 to 27°C as polymer concentration is increased from 0.8 to 5.5 wt% [1] [3]. It could be easily pictured that the polymer concentration should be locally higher on MSN surface, despite the low nanoparticle concentration (0.025 mg/mL). Thus, the densely packed pSBMA on MSN surface has a reduced distance between

chains compared to a free polymer solution. This reduction in conformational freedom due to steric hindrance contributes to the formation of more electrostatic interactions between molecules. Therefore, higher temperatures are required to break up these ionic attractions and allow a phase transition from a collapsed to a solubilized state. This result is opposite to that reported for silica-graft-pSBMA nanoparticles of 50 nm in diameter, when analyzed by DLS in aqueous solution [38]. Those authors showed a decreasing curve with a hydrodynamic radius dropping from 280 nm at 0°C to 150 nm at 66°C, and a reported UCST value of 53°C. This disagreement may be related to the four times higher nanoparticle concentration used for DLS solution, as well as the lower sizes of silica nanoparticles, and the six times higher pSBMA molecular weights used by the authors, compared with this study. All these factors would significantly increase the electrostatic interactions, favoring the formation of particle aggregates that could lead to an apparent decrease in size with a temperature augmentation. It is worth noting that hydrodynamic sizes measured by DLS (see Equation 1), are defined by means of the diffusion coefficient through the Brownian motion detected by the laser. Then, a grafted polymer shell, with the zwitterionic chains projecting out into the medium, will reduce the diffusion speed of the particles in solution, increasing the hydrodynamic diameter. Hence, the silica particle diameter, or core diameter, will be augmented by the presence of the zwitterionic chains, even if they are collapsed. But only an increment of the hydrodynamic size makes sense with the display of a UCST point, where a hydrated polymer layer is expected to be formed with temperature rising.

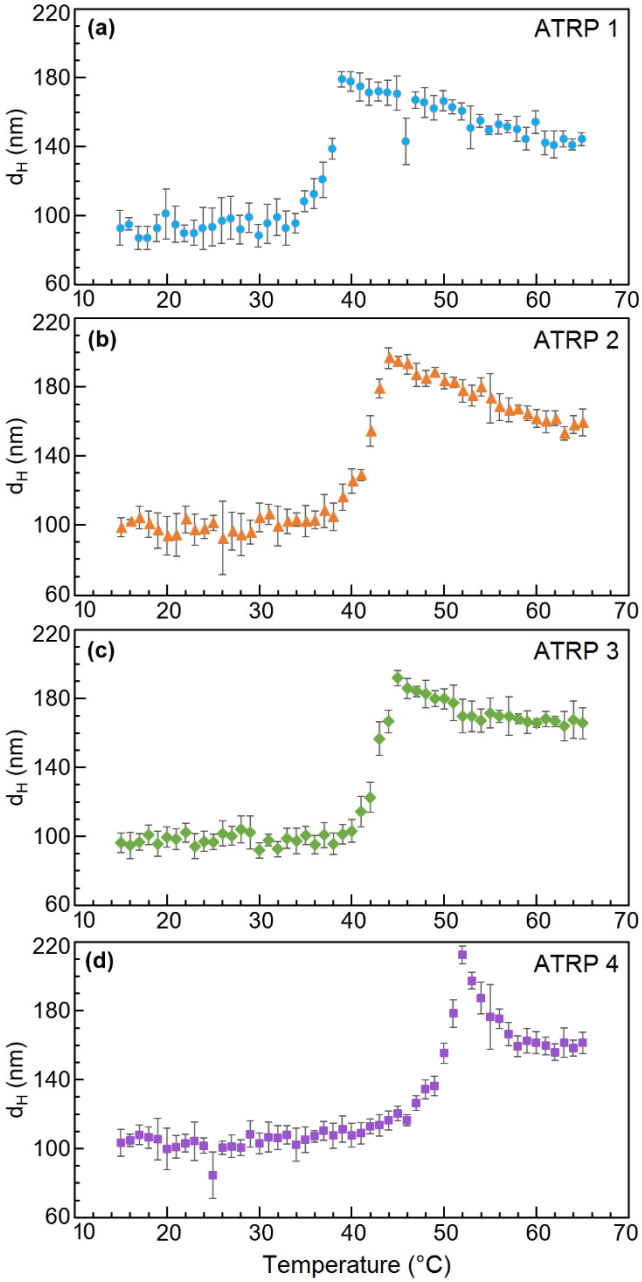

Figure 1. Variation of hydrodynamic particle diameter measured by DLS for pSBMA-MSN synthesized by increasing the functionalization time with the ATRP initiator (BrTEOS) to: a) 30 min, b) 4 h, c) 12 h and, d) 24 h (ATRP 1 to 4, using a constant SBMA/CuBr molar ratio of 50). Error bars represent one standard deviation.

Table II summarizes the transition temperatures and hydrodynamic diameters obtained for all experiments. For ATRP 1 to 4, during the first stage, the initial average hydrodynamic diameter ($d_{H,av}$) is very close to the particle diameter found by TEM (95 ± 15 nm), indicating the collapse of the zwitterionic chains on the silica surface. The second stage is then defined by an initial phase transition temperature

(T_i) and a maximum phase transition temperature (T_{max}). As shown in Figure 1 for ATRP 1 to 4, both T_i and T_{max} moved to the right. This may be explained by taking into account the molecular weight of the zwitterionic polymer attached on the nanoparticle, which is directly related to their chain length. The longer the polymer chain is, the higher the amount of electrostatic interactions among sulfobetaine groups, thus, the higher the energy required for its phase transition. Interestingly, a wider transition range of temperatures was achieved for the pSBMA-MSN product with the longest theoretical chain length (ATRP 4, Table I). Then, when enough energy is provided to weaken these ionic pairings, polymer chains gradually acquire a more extended polymer conformation until reaching a maximum value, $d_{H,max}$. This peak could be associated with an excess of entropy due to the thermal inertia of heating, which allows brush chains to gain thermal energy and extend in space. Likewise, this is favored by the polymer packing density and the steric effects. Since every chain is held and grafted by one extreme on MSN surface, they will organize by projecting and pointing out radially towards the solution, spreading to their maximum length. Once this limit is reached, they will tend to relax due to the entropic effects, modifying their length to a point given by their energetic state, until reaching a final value $d_{H,f}$ (between 10-30 nm lower than their $d_{H,max}$). ATRP 4 nanoparticles show the highest transition temperature and hydrodynamic size when products synthesized at a constant monomer/catalyst molar ratio are used (Tables I and II). This $d_{H,max}$ is related to the maximum theoretical chain calculated. Besides, for the ATRP 4 product, the highest decrease from the maximum ($d_{H,max}$) to the final size ($d_{H,f}$) was achieved during the third stage (51 nm, Table II). This rapid molecular relaxation is related with its long chain length, and low packing density, which provide much more space between chains, allowing them to acquire a less extended conformation. The variation of chain length with graft density is further analyzed [31].

Table II. Summary of transition temperatures and hydrodynamic sizes obtained by DLS for all pSBMA-MSN products.

	Transition temperatures (°C)		Hydrodynamic size, d_H (nm)		
ATRP	Initial (T_i)	Maximum (T_{max})	Initial average ($d_{H,av}$)	Maximum ($d_{H,max}$)	Final ($d_{H,f}$)
1	34	39	94	179	145
2	38	44	99	197	159
3	40	45	98	192	166
4	42	52	105	213	162
5	32	34	97	159	142
6	36	42	102	181	157
7	39	45	104	199	181
8	41	48	103	204	190
9	43	52	109	230	194

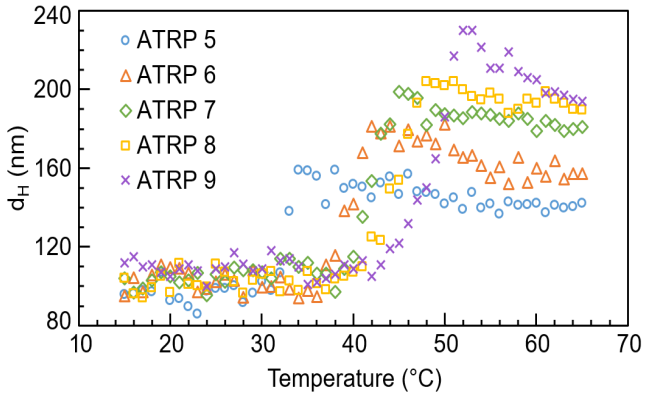

Figure 2. Variation of hydrodynamic particle diameter measured by DLS for pSBMA-MSN synthesized by increasing the SBMA/CuBr molar ratio to: a) 5, b) 25, c) 50, d) 100 and e) 150 (ATRP 5 to 9, using a constant functionalization time (1 h) with the ATRP initiator, BrTEOS).

When MSN nanoparticles were allowed to react for 1 hour with the BrTEOS initiator, and the ATRP reaction was then performed while varying the monomer/catalyst ratio, five additional products were synthesized (ATRP 5 to 9) [31]. Hydrodynamic sizes measured by DLS for these nanoparticles are shown in Figure 2, and their principal values summarized in Table II. As previously described in Figure1, similar curves are

observed in Figure 2, with initial particle diameters around 100 nm when the polymer layer is collapsed on the MSN surface. The average values were slightly lower for ATRP 5 ($d_{H,av}$ = 97 nm) and slightly higher for ATRP 9 ($d_{H,av}$ = 109 nm), as it could be expected from the molecular weights of their polymer layers. Moreover, a transition temperature range defining a second stage is observed, which moves to lower temperatures and widens from ATRP 5 to 9. Along these lines, the lowest initial transition temperature T_i was obtained for ATRP 5, while the highest T_i value was obtained for ATRP 9 (Table II). This trend is clearly related to the molecular weight of the products, which increases from 6 500 to 32 300 from ATRP 5 to 9, respectively. Therefore, the maximum point (T_{max}, $d_{H,max}$) observed in Figure 2 for each sample moves accordingly from the lowest value (34 °C , 159 nm) for ATRP 5 to the highest value (52°C, 230 nm) for ATRP 9.

Furthermore, due to the chain relaxation from this maximum stretching state, a decrease in particle size was also observed in all cases. It is worth noting that the functionalization time with BrTEOS was the same for all MSN samples, and that the polymerization kinetics depend directly on monomer concentration. Thus, higher graft densities were found when more monomer was available during the reaction (increasing the SBMA/CuBr molar ratio from 5 to 150, Table I). These graft density values along with the molecular weight and the estimated theoretical chains suggest that ATRP 5 product is the one with the thinner brush layer, while ATRP 9 product is the one with the thicker and denser one. For example, polymer chains from ATRP 9 would have less space and would suffer more steric effects, allowing them to radially stretch the most compared to all samples. Then, entropic effects would make the chain to recover to a more stable conformation, until reaching its final solubilized size. Consequently with this result, the lowest and highest final particle sizes $d_{H,f}$ (142 nm and 194 nm) were measured for the products with the lowest and the highest molecular weights (ATRP 5 and 9, respectively).

B. Influence of pH in the hydrodynamic diameter

Nanoparticle dispersions were prepared with different pH values ranging from 1 to 13, while temperature was kept constant at 30°C. The hydrodynamic sizes obtained from DLS followed the same trend for all products (ATRP 1 to 9), with d_H values

almost overlapped in all cases for each pH value tested. For the sake of clarity, only two representative samples were chosen, the products with the thinnest and the thickest polymer layers (ATRP 5 and 9, respectively), and their results are shown in Figure 3. It is observed that the variation of the hydrodynamic size of nanoparticles with pH may be defined in three regions. First, d_H decreases when pH value is increased from 1 to 4. Then, a constant d_H was determined for all samples with intermediate pH values from 5 to 9. Finally, a third region is observed where the tendency is inverted and d_H increases for high pH values (from 10 to 13).

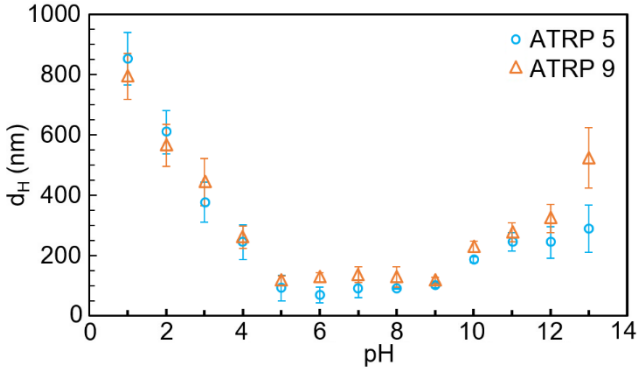

Figure 3. Variation of hydrodynamic particle diameter (by DLS) with pH value for pSBMA-MSN aqueous dispersions. Error bars represent one standard deviation.

In the first region (Figure 3), d_H values reach the micron-sized region, indicating the formation of nanoparticle aggregates in very acidic media. Thus, the advance of this aggregation state is proportionally diminished to the decrease of the pH value. In the same manner, in the third region, d_H values increase from around 200 to 600 nm. These tendencies are explained by the expansion of the chains due to the solvation of the quaternary ammonium and sulfonate groups of the polymer, according to the acidity or basicity of the medium. Instead, in a second region, the polymer layer exhibits its zwitterionic nature for pH values between 5 and 9. In this pH range, pSBMA molecules are in a less solvated state, since its formal positive and negative charges are balanced. In this manner, the lowest particle sizes were obtained in this region (around 100-110 nm), indicating the polymer chain collapse on the MSN surface. This is consistent with the values previously detailed for samples ATRP 5 and 9 when analyzed at 30°C (see Figure 2). It is important to notice that the aggregation state found for this experiment was evident for all dispersions, which showed a whitish and opaque appearance for pH values lower than 3 or higher than 12. This is further

indicated by the large error bars shown in Figure 3. At extreme values (0 and 14), DLS measurements could not be performed due to this high state of aggregation.

C. Influence of pH on zeta potential

In order to have a deeper understanding of the zwitterionic behaviour of pSBMA-MSN in aqueous solutions, the zeta potential (ZP) of all products was measured for different pH values (from 2 to 11). These results are shown in Figure 4 for ATRP 1 to 9, at a constant temperature (30°C). First, native MSN is compared with the reported value in the literature about amorphous silica [39], as shown in Figure 4a. Both curves present the same decreasing trend, as a result of the high concentration of hydroxyl groups. Accordingly, both curves reached very negative ZP values (around -75 mV), while crossing the axis at the same pH value (2.7). This is the isoelectric point of the silica, which is consistent with the expected value of around 1.45-3.50, depending on the acid used during silica synthesis [40]. In practice, this zero charge point (ZCP) is usually determined at a pH value between 2 and 3, depending on the type of silica (crystalline or amorphous) [39].

The variation of ZP with pH values for pSBMA-MSN nanoparticles synthesized in ATRP 1 was additionally studied, as shown in Figure 4a. This curve appears to be displaced upwards around 25 mV compared with the one of native MSN nanoparticles (without polymer layer). Besides, the ZCP is shifted to a pH value of 6. Hence, the product of ATRP 1 exhibits two ranges of ZP, which may be explained by taking into account the charges of the pSBMA layer. For pH values lower to 6, positive ZP values are caused by the protonation of the zwitterionic molecule (by quaternary ammonium groups, $(CH_3)N^+$). In contrast for pH values higher than 6, the deprotonation of the molecule (by sulfonate groups, SO_3^-) changes the particle charge to negative ZP values. The strength of these positive and negative groups of zwitterionic molecules affects ZP as well. Thus, sulfonate groups have a pKa value of 2, referred to strong acids, while tetramethylammonium groups ($–(CH_3)N^+$) have a pKb value of 5, indicating a weak base [41]. As a result, pSBMA-MSN particles exhibited a lower displacement from the zero charge axis at acidic conditions (with ZP values around +20 mV), while at basic conditions, a higher displacement of ZP values was reached (around -30V).

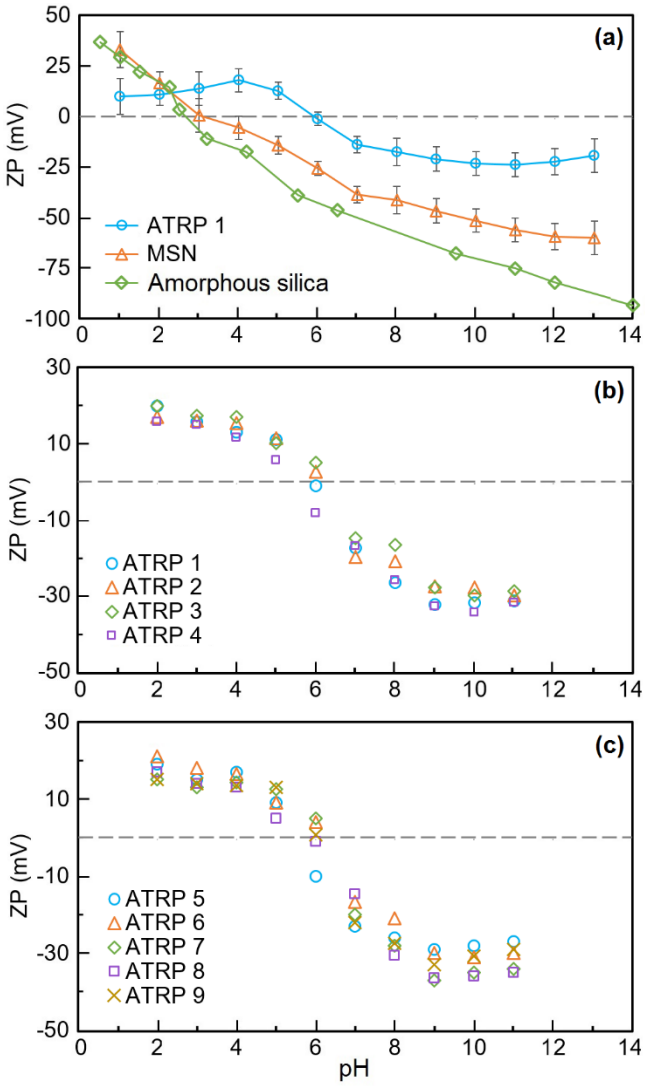

Figure 4. Zeta potential (ZP) variation with pH values for pSBMA-MSN products from: a) ATRP 1, compared with native MSN and amorphous silica, b) ATRP 1-4 and, c) ATRP 5-9. Error bars represent one standard deviation.

ZP measurements of all ATRP products are summarized in Figures 4b and 4c. Data reported for all samples is consistent with the behavior described for nanoparticles obtained from ATRP 1. The isoelectric point was calculated between 5.5 and 6.5 in all cases, corroborating the results shown in Figure 3, since all ZCP were determined in the zwitterionic range of the molecule, where both positive and negative charges are in equilibrium. Besides, no report was found about the influence of the shell thickness on zeta potential, *e.g.* the influence of the polymer molecular weight on the surface charge of the zwitterionic layer. In this study, the similarity of the results illustrated in Figure 4b and 4c are a clear indication that the polymer layer of all products is effective to modify the silica surface of MSN nanoparticles. Therefore, it is

possible to control the response of the zwitterionic macromolecules in solution, regardless of its morphological characteristics (polymer graft density and shell thickness). Results shown in Figure 4 are in agreement with those reported for nanoparticles modified with pSBMA or other zwitterionic molecules like amino acids. For example, the same decreasing trend of ZP with pH values was detailed in Au-capped MSN modified with L-cysteine for releasing an anticancer drug (ZCP at pH = 5) [42], self-aggregating pSBMA polymer nanoparticles for oral delivery systems (ZCP at pH = 5.2) [23], and L-lysine surface modified silica nanoparticles (SNP) (ZCP at pH=7) [11]. Moreover, the surface modification of SNP with other zwitterion such as poly(carboxymethylbetaine), or pCBMA was also reported with a ZP of -18.4 mV when dispersed in water [25]. In contrast, ZP results for pSBMA brushes grafted onto silica plates were determined to be independent of pH values [41]. This could be an evidence of the strong influence of the surface curvature on the packing density, the morphology of the brush and, hence4 on the electrical potential measured at the double layer formed at the surface of the different geometries.

D. Influence of temperature on zeta potential

In addition, the temperature response of pSBMA-MSN products was analyzed at neutral conditions (pH = 7), and the results are summarized in Figure 5. The ZP proportionally increases with temperature in all samples. This tendency may be explained by considering that all variables in Henry's Equation are temperature dependent (Equation 3). The strongest influence of temperature is seen for the viscosity (η), and it is inversely proportional to ZP. The higher the temperature, the lower the viscosity and therefore, the lower the ZP. However, the electrophoretic mobility (μ_E) is temperature dependent too if Joule's effect is taken into account, meaning an increase in μ_E by heat dissipation through the current flow. It is equally important that an increase in temperature further affects the dielectric constant (ε) by favoring the creation of dipoles and its orientation with the electric field. Finally, the influence of temperature on the Henry's function may be estimated through the Debye length (Equation 4). For example, a 50°C variation in temperature would only affects the second decimal place of the f(κa) value, making it reasonable to disregard its influence. Thus, in general, it is always expected that ZP values increase with

temperature [43], and it is predicted an increase rate of 0.34 %/°C for amorphous silica [44]. As shown in Figure 5a, a linear tendency (ZP = a + mT) was calculated for the results obtained from ATRP 1, which predicts an increase rate of 0.65 %/C. The minimum and maximum rates (0.50 and 0.87 %/°C) were found for ATRP 2 and ATRP 8. This higher rates for pSBMA-MSN products compared with those reported for silica materials were expected, due to the responsive nature of the zwitterionic brush.

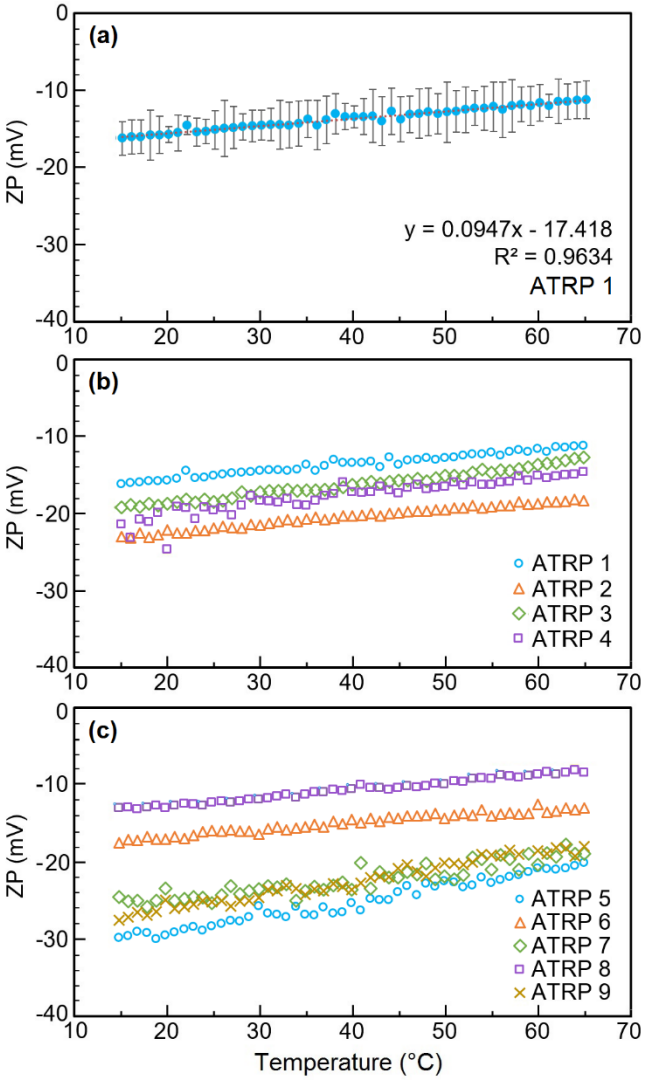

Figure 5. Zeta potential (ZP) variation with temperature (pH = 7) for pSBMA-MSN products from: a) ATRP 1, b) ATRP1-4 and, c) ATRP 5-9. Error bars represent one standard deviation.

As seen in Figure 5, there seems to be no apparent correlation between the ZP variation with temperature and the molecular weight of the polymer layers for each

pSBMA-MSN product (Table I). As expected, the hydrodynamic diameter (d_H) increases with temperature, as confirmed by the results shown in Figures 1 and 2. This increase in the thickness of polymer brush would affect the Henry's function, and hence the ZP value. For example, using the lowest (94 nm) and the highest (230 nm) d_H values obtained for ATRP 1 and 9, respectively (Table II), a variation of only 0.1 was found for $f(\kappa a)$ when calculated from Equation 5. But this fluctuation from $f(\kappa a)$ = 1.3 to $f(\kappa a)$ = 1.4 would only cause a change of ±3.5 mV on ZP. This small variation is in the uncertainty range of the measurement (see error bars in Figure 5a), leading to the conclusion that there is no evident influence of the thickness of polymer brushes on ZP. These results are dependent on the $f(\kappa a)$ values used, since d_H is *a priori* unknown and then, usually two extreme approximations are used. The Hückel approximation is used for small particle diameters (*e.g.* κa >1), and for low electrolyte concentration (<10^{-5}M) in non-polar media, leading to a value of $f(\kappa a)$= 1.0 [33]. The opposite consideration is the Smoluchowski approximation, $f(\kappa a)$= 1.5, used for bigger particles in aqueous solvent. Henry's function calculated by Equation 5 also changes depending on the pH value. For example, $f(\kappa a)$ values of 1.37 (d_H = 100 nm) or 1.43 (d_H = 230 nm) were obtained for acidic media (pH = 3), while $f(\kappa a)$ values of 1.25 (d_H = 100 nm) or 1.34 (d_H = 230 nm) were calculated for basic media (pH = 10). In this study, an average value of $f(\kappa a)$ = 1.35 was used throughout all experiments, except for those changing the electrolyte concentration, as explained below.

E. Influence of NaCl concentration on zeta potential

The modulation of ZP values to satisfy a specific need is very important when selecting the final application of pSBMA-MSN, e.g. as a drug carrier. For this purpose, the behavior of pSBMA brushes in the presence of an electrolyte such as sodium chloride was studied. Nine dispersions were prepared with each pSBMA-MSN product, modifying salt concentrations between 0 and 100 mM of NaCl in water. Results are summarized in Figure 6.

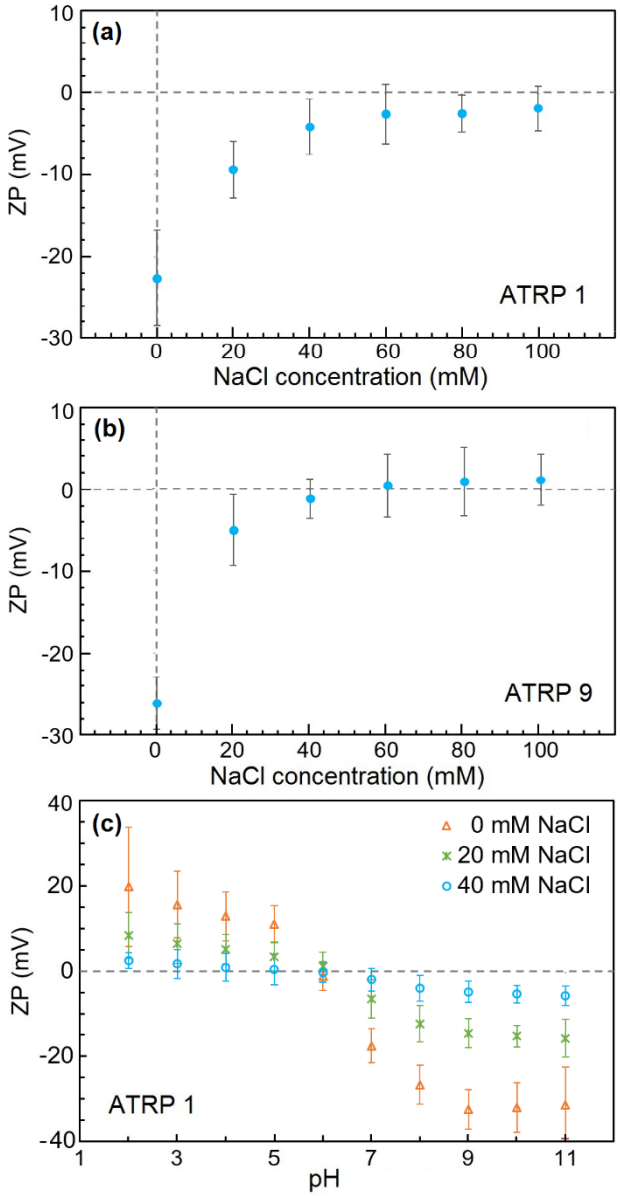

Figure 6. Zeta potential (ZP) variation with NaCl concentration for pSBMA-MSN products from: a) ATRP 1, b) ATRP 9 and, c) ZP variation with pH for ATRP 1 (T=30°C). Error bars represent one standard deviation.

For ATRP 1, Figure 6a shows a growing tendency of ZP when NaCl concentration is increased. This trend implies a stronger interaction between Na^+ and $–SO_3^–$, than that between $Cl^–$ and $–(CH_3)N^+$ ions [45]. Since interactions between the quaternary ammonium and the anion are weaker, ZP increases due to the preference of pSBMA to form a complex with the cation. Thus, Na^+ cations balance the anionic charge of the partially hydrolyzed zwitterionic chains, until reaching a final stabilized value near the isoelectric point. The tendency described for ATRP 1 (Figure 6a) was observed in all products, and ATRP 9 is shown as an example (Figure 6b). In all

cases, an initial ZP value around -20 and -30 mV was neutralized and reached a constant value when increasing NaCl concentration to 40-60 mM. This neutralization near the ZCP was expected for a sulfobetaine group, since it has a 1:1 relation between positive and negative charges. It is worth to notice that an excess in salt concentration could cause an opposite result to the anti-polyelectrolyte effect expected for zwitterionic molecules, since the excess ions would generate an osmotic pressure, causing chains to collapse [46]. As shown in Figures 6a and 6b, salt concentrations above 60 mM did not modify ZP values in any of the samples. This is in agreement with other reports using electrolyte concentrations of the same order of magnitude (15 mM NaCl [47] and 10 mM KCl [48]) to adjust ZP values of pSBMA brushes. Higher values are required to reach a constant ZP for pSBMA in solution (170 mM [45]), since more portions of the pSBMA chains are hindered in the grafted brush than those available for ion interaction when the polymer is free in the medium.

Finally, Figure 6c shows ZP variation in function of pH for different NaCl concentrations in ATRP 1. It is shown that, by changing the electrolyte concentration in the dispersion, it is possible to control the buffer capacity of the zwitterion, reaching an almost zero potential value for all the pH range. The same finding was observed in all the pSBMA-MSN products. It is important to notice that NaCl concentration causes $f(\kappa a)$ to increase significantly to values of 1.48 (d_H = 100 nm) and 1.49 (d_H = 230 nm). For this reason, the Smoluchowski's approximation was always used for ZP estimation in the presence of the electrolyte. In this way, the ZP can be modulated by controlling the ionic concentration of the media, to reach a certain profile required for a specific response, according to the final application of the carrier.

IV. CONCLUSIONS

The aqueous behaviour of pSBMA-MSN dispersions was studied by means of the hydrodynamic diameter and the zeta potential. It was demonstrated that polymer brushes were all temperature-responsive, since hydrodynamic diameter increased from 94-109 nm to 145-194 nm when temperature was varied from 15 to 65°C. This development may be attributed to a conformational change of the polymer chains,

which are collapsed on the MSN surface at low temperatures, giving for the pSBMA-MSN product a diameter close to the native MSN particle size (95 ± 15 nm). Then, as temperature increased, a transition state is reached where the energy requirements to break the electrostatic interaction between zwitterion molecules are overcome, allowing chain solvation. Thus, hydrodynamic diameter gradually increases until a maximum size and, due to entropic effects, the polymer chains relaxed until attaining a final particle size. Noticeably, the values of transition temperatures and final hydrodynamic diameters were found to be dependent on the molecular weight and theoretical length chain of polymer brushes. In addition, particle size in solution was studied for the pSBMA-MSN product, while varying pH of medium. Zwitterionic range was established for pH values of 5-9, which allowed both charges (from quaternary ammonium and sulfonate groups) to get balanced for the polymer brush. At lower and higher pH values from this range, particle aggregation was observed, causing a significant increase in the hydrodynamic diameter of the dispersed particles and reaching micron sizes.

Zeta potential of pSBMA-MSN dispersions was also analyzed, resulting in a very similar tendency for all products. Distinctly, positive ZP was measured for acidic media, while negative ZP were obtained for basic media, displaying an isoelectric point at a pH range of 5.5-6.5. Moreover, a directly proportional trend was found for ZP values with temperature. These results were independent of graft density or polymer layer thickness, evidencing that, for the purpose of zeta potential variations, polymer brushes with the different morphologies tested were all effective in particle surface modification. Finally, the anti-polyelectrolyte effect of zwitterions was corroborated and an electrolyte concentration of 40-60 mM of NaCl in aqueous solution was used to shift the zeta potential to near-zero charge values for all the products. Therefore, it was possible to modulate particle behaviour in solution by adjusting pH, temperature and ionic concentration of media. These results may be applied to achieve a specific response for pSBMA-MSN to be used in biomedicine or nanopharmaceutical fields, *i.e.* as carrier for controlled drug delivery applications. Further studies would involve the analysis of dispersions stability in different protein solutions to fully understand the poly-zwitterionic solution behavior for the development of novel and smart responsive layers.

ACKNOWLEDGEMENTS

José L. Gómez Ribelles acknowledges the support of the Ministerio de Economía y Competitividad, MINECO (research number MAT2016-76039-C4-1-R). CIBER-BBN is an initiative funded by the VI National R&D&I Plan 2008-2011, Iniciativa Ingenio 2010, Consolider Program, CIBER Actions and financed by the Instituto de Salud Carlos III with assistance from the European Regional Development Fund. This work was also supported by COLCIENCIAS (Departamento Administrativo de Ciencia Tecnología e Innovación, Convocatoria 567 Doctorados Nacionales) and Universidad Nacional de Colombia (grant number DIB 201010021438). The authors acknowledge the effort of Ramón Martínez Máñez, Scientific Director of the Biomedical Research Networking Center in Bioengineering, Biomaterials and Nanomedicine (CIBER-BBN), and Head of the Interuniversity Research Institute for Molecular Recognition and Technological Development (IDM) at Universitat Politècnica de València, where all measurements were performed.

REFERENCES

[1] A.Z. Mirza and F.A. Siddiqui, Int. Nano Lett. **4**, (2014).

[2] E. van Andel, Romantic Surfaces - Zwitterionic Polymer Brushes for Biomedical Applications, Doctoral Thesis, Wageningen University, 2018.

[3] D. Lombardo, M.A. Kiselev, and M.T. Caccamo, J. Nanomater. **2019**, 3702518 (2019).

[4] S. Salmaso and P. Caliceti, J. Drug Deliv. **2013**, 374252 (2013).

[5] Á.A. Beltrán-Osuna and J.E. Perilla, J. Sol-Gel Sci. Technol. **77**, 480 (2016).

[6] S. Bhattacharyya, H. Wang, and P. Ducheyne, Acta Biomater. **8**, 3429 (2012).

[7] H. Peng, R. Dong, S. Wang, Z. Zhang, M. Luo, C. Bai, Q. Zhao, J. Li, L. Chen, and H. Xiong, Int. J. Pharm. **446**, 153 (2013).

[8] P. Demuth, M. Hurley, C. Wu, S. Galanie, M.R. Zachariah, and P. Deshong, Microporous Mesoporous Mater. **141**, 128 (2011).

[9] C.Y. Lin, C.M. Yang, and M. Lindén, RSC Adv. **9**, 33912 (2019).

[10] G. Li, G. Cheng, H. Xue, S. Chen, F. Zhang, and S. Jiang, Biomaterials **29**, 4592 (2008).

[11] H. Wang, F. Cheng, W. Shen, G. Cheng, J. Zhao, W. Peng, and J. Qu, Acta Biomater. **40**, 273 (2016).

[12] V. V. Khutoryanskiy, Adv. Drug Deliv. Rev. **124**, 140 (2018).
[13] P. Dogra, N.L. Adolphi, Z. Wang, Y.S. Lin, K.S. Butler, P.N. Durfee, J.G. Croissant, A. Noureddine, E.N. Coker, E.L. Bearer, V. Cristini, and C.J. Brinker, Nat. Commun. **9**, 4551 (2018).
[14] L.D. Blackman, P.A. Gunatillake, P. Cass, and K.E.S. Locock, Chem. Soc. Rev. **48**, 757 (2019).
[15] D. Jana, S. Unser, I. Bruzas, and L. Sagle, in *World Sci. Encycl. Nanomedicine Bioeng. I*, edited by D. Shi (World Scientific Publishing Co. Pte. Ltd., 2017), pp. 103–150.
[16] C. Wu, Y. Zhou, H. Wang, and J. Hu, Nanomaterials **9**, 706 (2019).
[17] B.R. Knowles, D. Yang, P. Wagner, S. Maclaughlin, M.J. Higgins, and P.J. Molino, Langmuir **35**, 1335 (2019).
[18] S. Jiang, S. Chen, Y. Chang, and Z. Zhang, US Patent 598544 B2 (2017).
[19] K. Matyjaszewski and J. Spanswick, *Atom Transfer Radical Polymerization* (Elsevier B.V., 2012).
[20] Y. Chang, W.Y. Chen, W. Yandi, Y.J. Shih, W.L. Chu, Y.L. Liu, C.W. Chu, R.C. Ruaan, and A. Higuchi, Biomacromolecules **10**, 2092 (2009).
[21] Y. Zhao, T. Bai, Q. Shao, S. Jiang, and A.Q. Shen, Polym. Chem. **6**, 1066 (2015).
[22] Y. Zhou, P. Dong, Y. Wei, J. Qian, and D. Hua, Colloids Surfaces B Biointerfaces **132**, 132 (2015).
[23] C.Y. Chen and H.L. Wang, Macromol. Rapid Commun. **35**, 1534 (2014).
[24] V.A. Vasantha, W. Rusli, C. Junhui, Z. Wenguang, K.V. Sreekanth, R. Singh, and A. Parthiban, RSC Adv. **9**, 27199 (2019).
[25] H. Suzuki, M. Murou, H. Kitano, K. Ohno, and Y. Saruwatari, Colloids Surfaces B Biointerfaces **84**, 111 (2011).
[26] Z. Dong, J. Mao, D. Wang, M. Yang, W. Wang, S. Bo, and X. Ji, Macromol. Chem. Phys. **215**, 111 (2014).
[27] J. Zhu, X. Zhao, and C. He, RSC Adv. **5**, 53653 (2015).
[28] I.-T. Teng, Y.-J. Chang, L.-S. Wang, H.-Y. Lu, L.-C. Wu, C.-M. Yang, C.-C. Chiu, C.-H. Yang, S.-L. Hsu, and J.A. Ho, Biomaterials **34**, 7462 (2013).
[29] J.T. Sun, Z.Q. Yu, C.Y. Hong, and C.Y. Pan, Macromol. Rapid Commun. **33**, 811 (2012).
[30] S. Khatoon, H.S. Han, M. Lee, H. Lee, D.W. Jung, T. Thambi, M. Ikram, Y.M. Kang, G.R. Yi, and J.H. Park, Acta Biomater. **40**, 282 (2016).

[31] Á.A. Beltrán-Osuna, J. Ródenas-Rochina, J.L. Gómez Ribelles, and J.E. Perilla, Polym. Adv. Technol. **30**, 688 (2019).
[32] Á.A. Beltrán-Osuna, J.L. Gómez Ribelles, and J.E. Perilla, J. Nanoparticle Res. **19**, 381 (2017).
[33] S. Bhattacharjee, J. Control. Release **235**, 337 (2016).
[34] B.J. Kirby and E.F. Hasselbrink, Electrophoresis **25**, 187 (2004).
[35] J. Kim and D.F. Lawler, Bull. Korean Chem. Soc. **26**, 1083 (2005).
[36] Y.L. Khung and D. Narducci, Adv. Colloid Interface Sci. **226**, 166 (2015).
[37] Y.J. Shih and Y. Chang, Langmuir **26**, 17286 (2010).
[38] Z. Dong, J. Mao, D. Wang, M. Yang, W. Wang, S. Bo, and X. Ji, Macromol. Chem. Phys. **215**, 111 (2014).
[39] J.A. Alves Júnior, J. Baptista Baldo, J. Antonio, A. Júnior, and J.B. Baldo, New J. Glas. Ceram. **4**, 29 (2014).
[40] C.J. Brinker and G.W. Scherer, in *Sol-Gel Sci. Phys. Chem. Sol-Gel Process.* (Academic Press, Inc., 1990), p. 377.
[41] S. Guo, D. Jańczewski, X. Zhu, R. Quintana, T. He, and K.G. Neoh, J. Colloid Interface Sci. **452**, 43 (2015).
[42] X. Chen, X. Cheng, A.H. Soeriyadi, S.M. Sagnella, X. Lu, J.A. Scott, S.B. Lowe, M. Kavallaris, and J.J. Gooding, Biomater. Sci. **2**, 121 (2014).
[43] R. Venditti, X. Xuan, and D. Li, Microfluid. Nanofluidics **2**, 493 (2006).
[44] C.J. Evenhuis, R.M. Guijt, M. Macka, P.J. Marriot, and P.R. Haddad, Electrophoresis **27**, 672 (2006).
[45] M. Du, Y. Ma, H. Su, X. Wang, and Q. Zheng, RSC Adv. **5**, 33905 (2015).
[46] Y.Y. Jhan and R.Y. Tsay, J. Taiwan Inst. Chem. Eng. **45**, 3139 (2014).
[47] P. Liu and J. Song, Biomaterials **34**, 2442 (2013).
[48] L. Ni, J. Meng, G.M. Geise, Y. Zhang, and J. Zhou, J. Memb. Sci. **491**, 73 (2015).